

# Unsteady flow around impacting bluff bodies

T. Leweke<sup>a,\*</sup>, L. Schouveiler<sup>a</sup>, M.C. Thompson<sup>b</sup>, K. Hourigan<sup>b,c</sup>

<sup>a</sup>*Institut de Recherche sur les Phénomènes Hors Équilibre – CNRS, École Centrale, Aix-Marseille Université, 49 rue Frédéric Joliot-Curie, B.P. 146, F-13384 Marseille Cedex 13, France*

<sup>b</sup>*Fluids Laboratory for Aeronautical and Industrial Research, Department of Mechanical and Aerospace Engineering, Monash University, Victoria 3800, Australia*

<sup>c</sup>*Division of Biological Engineering, Monash University, Victoria 3800, Australia*

Received 25 July 2008; accepted 6 August 2008

---

## Abstract

The flow resulting from the collision without rebound of generic bluff bodies with a wall in a still viscous fluid is investigated both computationally and experimentally. Emphasis is on the case of a circular cylinder impact (two-dimensional geometry), but comparisons with the flow generated by the impact of a sphere (axisymmetric geometry) are included. For normal cylinder impacts, the two counter-rotating vortices forming behind the body during its motion continue their trajectory towards the wall after the collision, leading to the generation of opposite-signed secondary vorticity at the cylinder and wall surfaces. Secondary vortices forming from this vorticity at higher Reynolds numbers exhibit a short-wavelength three-dimensional instability. Comparison with the sphere impact reveals significant differences in the scales of the vortices after the collision, due to the additional vortex stretching acting in the axisymmetric geometry. This leads to a delay in the onset of three-dimensionality and to a different instability mechanism. Oblique cylinder impacts are also considered. For increasing impact angles, the wall effect is gradually reduced on one side of the cylinder, which favours the roll-up of the secondary vorticity and increases the rebound height of the vortex system.

© 2008 Elsevier Ltd. All rights reserved.

*Keywords:* Bluff bodies; Wall impact; Unsteady flow; Axisymmetric versus two-dimensional flow; 3D instability

---

## 1. Introduction

A solid body colliding with a solid surface is a common situation in many industrial and environmental applications, involving complex energy exchanges. One example, which is of importance to climate studies, is the resuspension of particles deposited on a surface (dust on the ground, sediments in rivers) by the impact of an object or other particles [see, e.g., Willetts (1998) and Ziskind (2006), for reviews on this topic]. Particle resuspension from a surface can be induced by two main mechanisms: (i) by ballistic ejection, where the collision of the impacting body breaks the bonds between the particles and transfers some of its kinetic energy to them (Rice et al., 1996; Shao et al., 1993); and (ii) by hydrodynamic effects, whereby the vortical structures generated by the impacting body in the surrounding fluid near the

---

\*Corresponding author. Tel.: +33 4 9613 9761; fax: +33 4 9613 9709.

E-mail address: [Thomas.Leweke@irphe.univ-mrs.fr](mailto:Thomas.Leweke@irphe.univ-mrs.fr) (T. Leweke).

wall entrain and lift up the deposited particles (Eames and Dalziel, 2000). The present paper deals with aspects related to the second purely hydrodynamic mechanism.

A further application can be found in the modelling of wall effects in particle-laden flows. Two-phase flows near walls are found, e.g., in fluidised-bed heat exchangers, where the flow generated by a particle impact locally modifies/enhances the heat exchange properties of the wall (forced convection). For the purpose of developing reliable models allowing numerical simulations of these flows, an understanding of the fundamentals of fluid–particle flows is needed. For the description of the bulk flow, studies such as the one by Zhang et al. (1999) have considered single particle–particle collisions in a viscous fluid. Fundamental studies of the hydrodynamics of particle–wall collisions include the ones by Eames and Dalziel (2000) and Gondret et al. (2002), with emphasis on dust resuspension and particle rebound, respectively. Leweke et al. (2004, 2006) and Thompson et al. (2007) have investigated in detail the unsteady flow resulting from the normal wall impact of a sphere, revealing the existence of axisymmetric and three-dimensional vortical structures, which could be explained by a centrifugal instability mechanism.

The present paper focusses again on the hydrodynamics associated with the impact of a bluff body on a wall. It represents a synthesis and an extension of previous work by Thompson et al. (2006, 2007). We investigate experimentally and numerically the flow induced by the normal or oblique collision of a circular cylinder with a wall at moderate Reynolds numbers. This configuration is a further idealisation of a particle–wall impact; however, as will be shown, comparison with the axisymmetric sphere impact case allows the identification of special features associated with the latter, and gives information about the validity of two-dimensional approaches for the study of fundamental particle–wall interactions.

After the description of the numerical methodology and the experimental procedure in Section 2, results concerning normal and oblique cylinder impacts are presented in Section 3, including comparison with the axisymmetric sphere impact. Conclusions are given in Section 4.

## 2. Methodology

### 2.1. Parameter definitions

The flow resulting from the collision without rebound of a circular cylinder (or a sphere) on a wall in a still viscous fluid is investigated. The body is impulsively started from rest, travels a distance  $L$  through the fluid at a constant velocity  $U$  towards a wall, then stops at the moment of contact with the wall. The parameters characterising such a configuration (see Fig. 1(a)) are the nondimensional running distance  $L/D$  and the Reynolds number  $Re = UD/\nu$ , where  $D$  is the body diameter and  $\nu$  the kinematic viscosity of the fluid. When oblique collisions are investigated, the angle  $\alpha$  between the body trajectory and the direction normal to the wall represents a third parameter.

In the present study, we focus on conditions without vortex shedding at the time of impact, with either two symmetric straight vortices of opposite sign behind the cylinder, or an axisymmetric vortex ring attached to the sphere. Since the

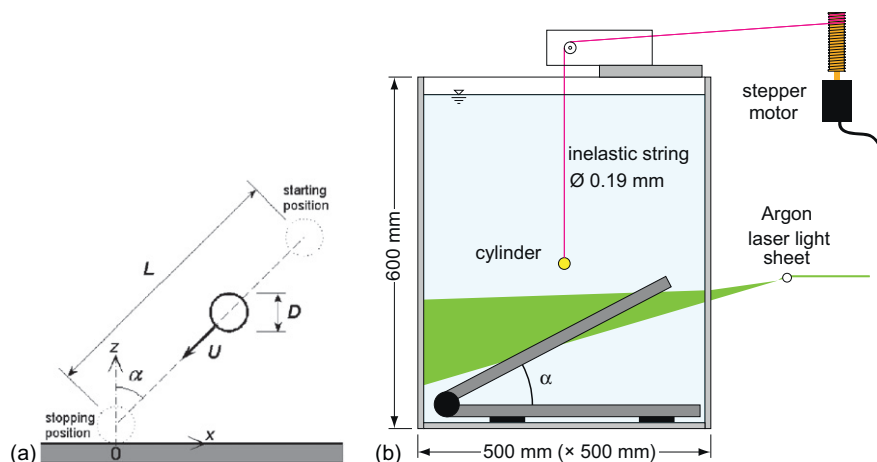


Fig. 1. (a) Problem definition and parameters; (b) experimental setup.

experiments and simulations are performed for Reynolds numbers above the critical values for the transition to unsteadiness of the asymptotic wake flow ( $Re \approx 50$  and  $270$  for the cylinder and sphere, respectively), such initial conditions require that the impact occurs while the wakes are still in a symmetric transient state. This imposes a limitation on the running lengths  $L/D$  to be used; they have to be short enough for the wake to remain symmetric, but also large enough for a well-defined recirculation region to develop behind the body. Preliminary experiments have shown that these conditions are met for values of  $L/D$  between 3 and 6.

Cartesian coordinates attached to the wall are used as defined in Fig. 1(a), with the origin given by the body impact point. Time  $t$  is non-dimensionalised using the characteristic advection time:  $\tau = t/(D/U)$ , with  $\tau = 0$  corresponding to the time of impact.

## 2.2. Numerical method

The numerical approach for investigating the two- and three-dimensional hydrodynamics associated with the impact of a particle on a wall is based on the spectral-element method incorporating a deforming mesh. The mesh points move towards the wall in a prescribed manner to minimise mesh distortion. Nevertheless, the solution still needs to be periodically remapped to a new mesh in order to reduce some negative effects, such as the reduction in time step due to local mesh compression. Remapping of the solution variables between meshes is performed using the same local spectral interpolation consistent with the spectral-element method, thus maintaining the inherent spatial accuracy. Temporal accuracy is second-order for the velocity field, due to the use of first-order boundary conditions for the pressure (Karniadakis et al., 1991). For the simulations of cylinder impact at a non-normal angle to the wall, the problem is treated in a frame moving tangentially to the wall so that the motion of the cylinder is normal to the wall in that frame of reference. The time-stepping method and spatial discretisation are described in Ryan et al. (2007) and Thompson et al. (1996). More details on the treatment of the moving mesh are given in Thompson et al. (2006).

## 2.3. Experimental details

Experiments were conducted in a 600 mm high glass tank with a square horizontal cross-section of  $500 \times 500 \text{ mm}^2$ , filled with water and equipped with a plexiglas false floor. For the cylinder impact, an aluminium rod of length 368 mm and diameter  $D = 15.9 \text{ mm}$  (aspect ratio of 23) was used, which was suspended horizontally by two inelastic threads, one at each end. The threads passed over a pulley and wrapped around a reel driven by a computer controlled stepper motor. The experimental setup is schematically shown in Fig. 1(b). This mechanism allowed lowering the body with a specified velocity  $U$ , and impulsively stopping the descent at the position of contact with the wall. Constant-velocity motion of the cylinder was chosen for simplicity, in order to keep the number of parameters governing the flow small. For the running lengths considered in this study (less than 7 diameters), three-dimensional effects related to the free ends of the body only propagated over a short axial distance, whereas the flow over most of the central part remained two-dimensional up to impact.

Oblique cylinder impacts, whereby the cylinder still touches the wall simultaneously over its entire length, were obtained using the same vertical body motion, but inclining the surface with which it collides. A second plexiglas plate was attached to the false floor in the tank using a swivel articulation (see Fig. 1(b)), allowing for a continuous variation of the inclination angle  $\alpha$ . In the present study, five angles between  $\alpha = 0$  (normal impact) and  $\alpha = 62^\circ$  were considered.

Qualitative and quantitative information about the evolution of the vortical structures of the flows generated by the bluff body impacts was obtained from dye visualisation. The body was coated with a solution of green fluorescent dye prior to lowering it into the water, and the patterns created by the dye entrained by the flow were illuminated by a vertical sheet of light from an argon ion laser passing through the body center. Visualisations were recorded with a digital video camera aligned perpendicular to the light sheet.

## 3. Results

### 3.1. Normal impact of a cylinder

We first consider the two-dimensional normal impact of a cylinder on a solid surface. Experiments were performed with a running length  $L/D = 4$  at a Reynolds number  $Re = 200$ , which is low enough for the flow to remain two-dimensional (i.e., independent of the direction of the cylinder axis, except near the cylinder ends). Numerical results were obtained using the two-dimensional version of the spectral-element code.

Fig. 2 shows a series of experimental dye visualisations and axial vorticity fields obtained from numerical simulations. The two sets of figures are drawn to the same scale and represent the same instants in time. We first note the excellent agreement between experiment and simulation, including even the smaller details of the flow, which validates each of the two approaches. The dye patterns clearly reveal the vortical structures during the time interval covered by Fig. 2. It was shown in Thompson et al. (2007) that noticeable deviations between the locations of dye and vorticity of the main vortical structures occur only at times beyond  $\tau \approx 20$ , due to the difference in the diffusion coefficients for dye and vorticity.

While the cylinder approaches the wall, dye washing off the cylinder surface is entrained into the two longitudinal opposite-signed vortices forming in its wake. These primary vortices can be seen at the instant of the impact ( $\tau = 0$ ) in Fig. 2(a). After the impact, Figs. 2(b–d) show that the two primary vortices continue to move towards the wall due the inertia of the cylinder wake. They travel along the sides of the cylinder and then horizontally outwards along the wall, which, using inviscid theory, can be interpreted as a motion induced by the image vortices inside the cylinder and wall. This motion induces secondary vorticity on the cylinder surface, which rolls up to form a secondary longitudinal vortex of opposite sign on each side of the cylinder, as seen in Fig. 2(b). The numerical results show another source of secondary vorticity in the viscous boundary layer at the wall (this vorticity is not visualised in the experiments due to the absence of dye on the wall surface). The secondary vorticity induces a slight upward motion (rebound) on the primary wake vortices, and then rolls around the latter as time increases. At  $\tau = 15$ , the two primary vortices have separated by a distance of around  $5D$ , and rebound to a height of around  $1.5D$ . Their characteristic core diameter is close to one cylinder diameter. From this time on, the flow slowly dies out, with the primary and secondary vorticity cancelling each

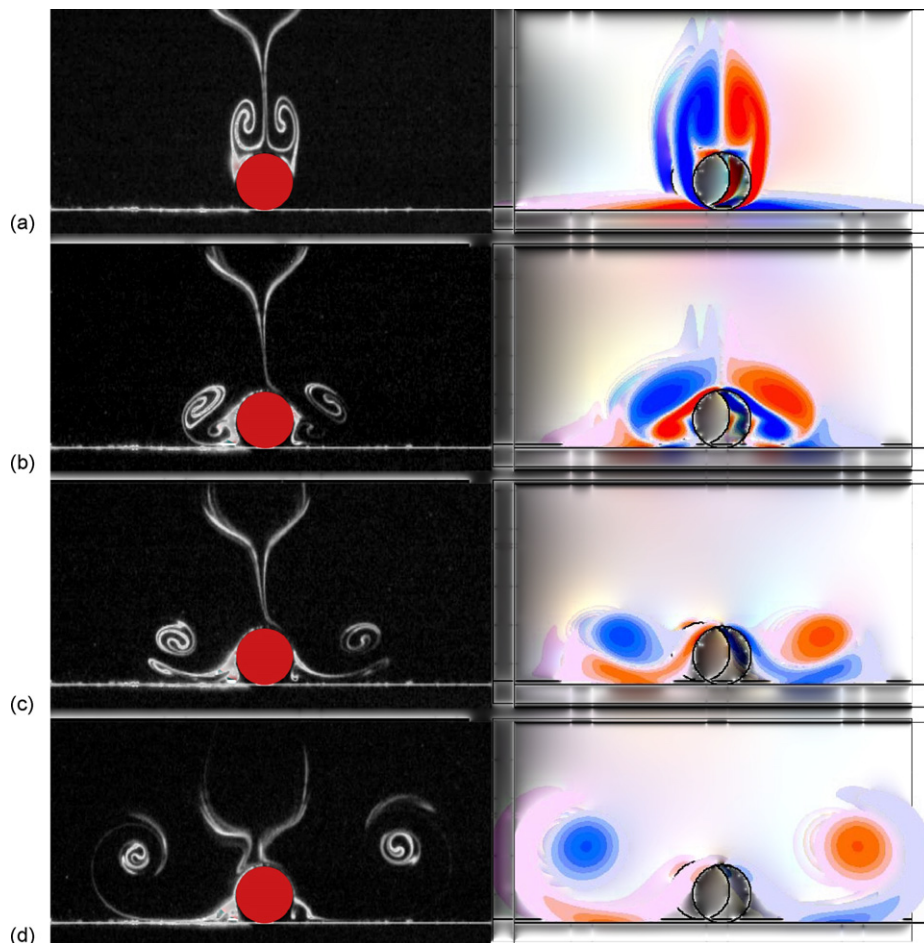


Fig. 2. Experimental dye visualisations (left) and vorticity field from numerical simulations (right) after the normal impact ( $\alpha = 0$ ) of a cylinder with a wall for  $Re = 200$  and running distance  $L/D = 4$ . (a)  $\tau = 0$ , (b)  $\tau = 2.1$ , (c)  $\tau = 4.9$ , (d)  $\tau = 15.1$ .

other by cross-diffusion. The dye visualisations and numerical simulations show that the planar symmetry with respect to the plane  $x = 0$  (see Fig. 1(a)) is preserved during the entire evolution of the flow for a normal impact of a circular cylinder in this low-Reynolds number regime.

For higher (but still moderate) Reynolds numbers, the flow around an impacting cylinder is still two-dimensional at the time of contact with the wall. However, the flow becomes three-dimensional during the later stages of its evolution. In Fig. 3, the vortical structures existing at  $\tau = 11$  in the flow resulting from a cylinder impact at  $Re = 400$  are shown. This result was obtained from three-dimensional simulations, in which a low-level white noise was added to the initially two-dimensional “base flow”. At this Reynolds number, the secondary vorticity from the cylinder and wall surfaces does not wrap around the primary vortex in a sheet-like structure as seen in Fig. 2 for lower  $Re$ . Instead, a concentrated secondary vortex is formed, which orbits around the primary one, and which undergoes a three-dimensional core instability, clearly visible in Fig. 3. The axial wavelength of this instability is about one cylinder diameter. A similar phenomenon was observed by Moet (2003), who simulated the interaction of a counter-rotating vortex pair with a wall. In this case, too, secondary vorticity from the wall is lifted up and rolls up into secondary vortices, which are three-dimensionally unstable. Moet (2003) identified this as the consequence of the so-called elliptic instability (Kerswell, 2002), found in flows with elliptic streamlines such as vortex cores exposed to an external strain field generated, e.g., by a second nearby vortex. The structure and wavelength of the perturbation observed on the secondary vortices in Fig. 3 are consistent with this instability mechanism.

### 3.2. Comparison with normal sphere impact

The axisymmetric configuration of a sphere impacting a wall in the normal direction has been investigated in detail by Thompson et al. (2007). In this section we present a direct comparison between the above results for the two-dimensional cylinder impact configuration and the corresponding axisymmetric cases from the sphere impact study.

In Fig. 4, the flows without three-dimensional instability at low  $Re$  are compared for the two different geometries, but otherwise identical parameters:  $Re = 200$  and  $L/D = 4$ . Whereas the distribution of azimuthal vorticity in the sphere geometry at impact ( $\tau = 0$ ) looks very similar to the axial vorticity field for the cylinder, significant differences are seen as the flow evolves after the collision. The primary wake vortices on each side of the sphere, which form a vortex ring, have a much smaller diameter of only about  $D/3$ . In addition, the late-time lateral spacing (i.e., the diameter of the primary vortex ring) is only about  $2D$ , compared to the  $5D$  separation for the cylinder geometry. Finally, the primary vortex hardly rebounds at all, and the magnitude of its vorticity decreases much faster than in the two-dimensional case.

The main reason for these differences is the presence of vortex stretching in the axisymmetric geometry. After the stop of the sphere motion, the vortex ring that has developed in its wake continues its downward motion and is forced to increase its diameter/perimeter considerably in order to slip around the sphere. This increase in length through motion in the positive radial direction is accompanied by an increase of the vorticity and a decrease of the core diameter, which are common features associated with vortex stretching. Both effects enhance the vorticity gradients in the meridional

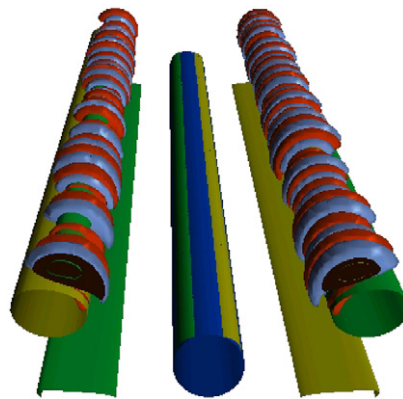


Fig. 3. Three-dimensional flow after the normal collision of a cylinder with a wall for  $Re = 400$  and  $L/D = 5$  at  $\tau = 11$ , from numerical simulation: isosurfaces of the spanwise vorticity, showing the primary vortices, and of the perturbation axial vorticity showing the short-wavelength instability developing on the orbiting secondary vortex. In addition, the position of the cylinder is shown and the wall vorticity beneath the primary cores can be seen. From Thompson et al. (2006).

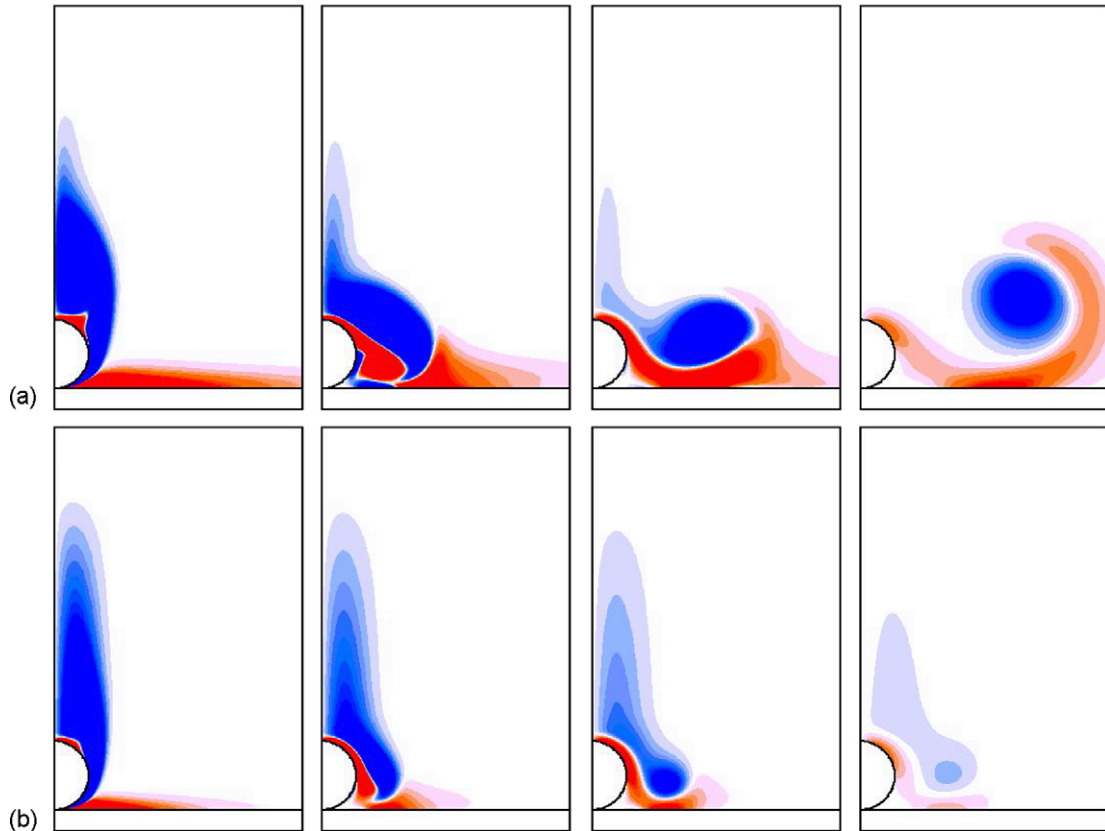


Fig. 4. Comparison between two-dimensional and axisymmetric flow for  $Re = 200$  and  $L/D = 4$ , from numerical simulation. (a) Axial vorticity after a cylinder impact; (b) azimuthal vorticity after a sphere impact. Colour scales are identical in absolute values; the scale in (a) was inverted for better visual comparison.

plane, and accelerate the diffusion and cross-annihilation of primary and secondary wall vorticity as the flow evolves, which explains the accelerated decrease of circulation, observed in Fig. 4.

These differences in the flow evolution also have consequences for the development of three-dimensional instabilities. Whereas for the cylinder impact, Fig. 3 shows the existence of an elliptic instability of the rolled-up secondary vortex at  $Re = 400$ , the flow remains entirely axisymmetric up to  $Re \simeq 1000$  for the sphere impact. As shown in Thompson et al. (2007), the destabilisation observed at higher  $Re$  is caused by a centrifugal instability (Bayly, 1988) of the primary vortex ring, with a wavelength (in the azimuthal direction) of only about  $D/3$ . Again, these differences in instability threshold and wavelength can be understood by the presence of stretching and the associated modifications of the primary vortex for the sphere impact case. The increased cross-diffusion of vorticity reduces the primary circulation  $\Gamma_p$ , and therefore also the primary vortex Reynolds number  $\Gamma_p/\nu$ . In addition, since the elliptic instability perturbation modes scale on the vortex core size, the reduced core diameter leads to smaller unstable wavelengths, which are subject to higher viscous damping. Both effects tend to delay the inception of three-dimensional instability to higher Reynolds numbers. Moreover, the vorticity distributions at the onset of instability are qualitatively different for the two configurations, which explains the different mechanisms leading to instability. They are compared in Fig. 5. Whereas the secondary vorticity developing after the cylinder impact rolls up into a concentrated vortex, subject to elliptic instability, it forms a rather uniform sheet wrapping around the primary vortex after the sphere impact, which generates a flow configuration which is centrifugally unstable. Fig. 5 also shows again the significant difference in cross-sectional scale.

### 3.3. Oblique impact of a cylinder

In this section, the flow resulting from an impact of a cylinder on a solid surface is presented. Experiments were carried out with four different impact angles  $\alpha$  (see Fig. 1(a) for the definition), considering only the two-dimensional low- $Re$  regime.

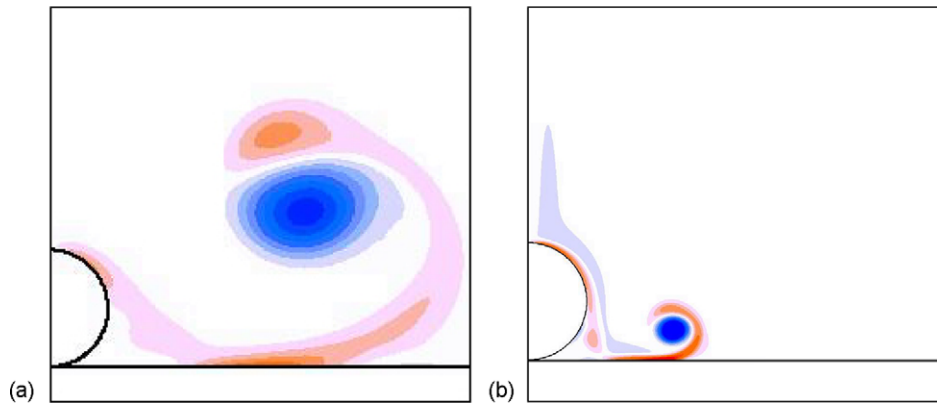


Fig. 5. Base flow for the conditions exhibiting three-dimensional instability, obtained by numerical simulation. (a) Two-dimensional flow for the cylinder impact: axial vorticity at  $\tau = 11$ , for  $Re = 400$  and  $L/D = 4$ . (b) Axisymmetric flow for the sphere impact: azimuthal vorticity at  $\tau = 4$ , for  $Re = 1200$  and  $L/D = 5$ .

The main features of the flow induced by an oblique cylinder impact are illustrated in Fig. 6 for the intermediate collision angle  $\alpha = 33^\circ$ ,  $Re = 200$  and  $L/D = 5$ . The figure shows a time series of experimental dye visualisations and numerically simulated distributions of axial vorticity. Note that the images from experiments, where the cylinder actually moves vertically, have been rotated by the angle  $\alpha$  to facilitate comparison with the numerical simulation and the normal-impact case shown in Fig. 2. As for the latter case, we again observe an excellent agreement between the two sets of results.

The flow state at the impact time  $\tau = 0$  (Fig. 6(a)) is very similar to the one for normal impact (Fig. 2(a)). It consists of two well-formed primary vortices attached behind the cylinder, which are almost perfectly symmetric with respect to the cylinder trajectory. This symmetry is lost after the impact, as seen in the post-collision snapshots of Figs. 6(b–d).

The flow evolution on the “right” side, below the cylinder trajectory and for  $x > 0$ , is qualitatively similar to the one observed for normal impact. The primary wake vortex passes by the cylinder, moves along the wall and lifts up, while a sheet of secondary vorticity from the cylinder and wall surfaces wraps around it. The vorticity distributions at  $\tau = 15.1$  for both cases (right halves of Figs. 2(d) and 6(d)) are almost identical.

On the contrary, the flow on the “far” side of the impact line ( $x < 0$ ) is strongly modified by the non-zero collision angle. Due to the inclined cylinder trajectory, the primary wake vortex feels the influence of the wall later than for the case of a normal trajectory. As it passes by the cylinder, the secondary vorticity generated at the surface of the latter has now time to roll-up into a concentrated secondary vortex, instead of combining with the wall vorticity to form a sheet-like structure. In fact, very little wall vorticity is generated on this side of the cylinder, compared to the opposite one, as seen in Figs. 6(c–d). Primary and secondary vortices then form an asymmetric vortex pair (dipole), which has a self-induced velocity leading to the enhanced rebound of the structure. For normal cylinder impacts, the formation of a concentrated secondary vortex was observed only at much higher Reynolds numbers, where it opened up the possibility for three-dimensional instability. For the oblique impact at low  $Re$ , this aspect has not been investigated further so far.

The lift-up and rebound of the dipole structure is further illustrated by the trajectories of the primary “left” vortex. In Fig. 7, the experimental measurements of these trajectories for the different impact angles are compiled. In Fig. 7(a), they are plotted in the frame of reference of the wall. This plot clearly shows how, as  $\alpha$  increases, the trajectories move away from the wall. The final rebound height varies from about  $1.5D$  for normal impact ( $\alpha = 0$ ) to twice this value for  $\alpha = 62^\circ$ . Fig. 7(b) shows the primary vortex paths in a representation where the cylinder trajectory is fixed. In this body-based reference frame, the initial trajectories are identical for all impact angles, up to a nondimensional time of about 2. They are almost straight, at an angle of about  $30^\circ$  to the cylinder path. The higher the impact angle, the longer the primary vortex remains on this common trajectory. After forming the dipole with the secondary vorticity from the cylinder surface, the primary vortex continues along a trajectory curved upwards, which indicates that its circulation is larger than the one of the secondary vortex. This difference appears to decrease for more oblique impacts, since the curvature of the dipole paths diminishes. Sheard et al. (2007) have investigated the flow resulting from a cylinder stopping away from a wall in mid-fluid. This situation is approached on the “far” side of the present configuration, as the impact angle reaches large values. For low Reynolds numbers, and running distances of the same order as considered here, Sheard et al. (2007) observed an almost straight trajectory of the primary vortex after the stopping of the body, indicating that the primary and secondary vortices have very similar circulations, which is consistent with the

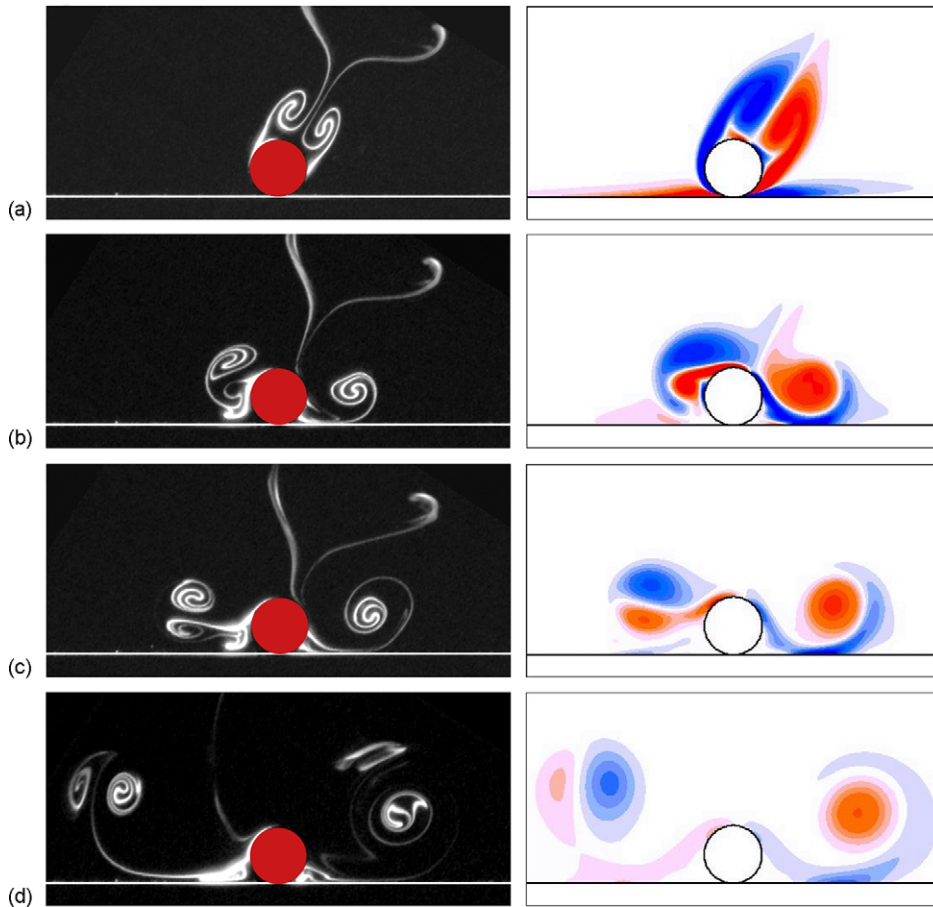


Fig. 6. Experimental dye visualisations (left) and vorticity field from numerical simulations (right) after the oblique collision ( $\alpha = 33^\circ$ ) of a cylinder with a wall for  $Re = 200$  and running distance  $L/D = 5$ . (a)  $\tau = 0$ , (b)  $\tau = 2.1$ , (c)  $\tau = 4.9$ , (d)  $\tau = 15.1$ .

trend observed in Fig. 7(b). (Other much more curved trajectories could also be found for different parameter combinations, in particular higher  $Re$ .)

#### 4. Concluding remarks

In this paper, we have presented experimental and numerical results concerning the flow around a circular cylinder impacting a solid wall. For normal impacts at low Reynolds numbers, the attached counter-rotating vortices, forming in the wake of the cylinder during its motion, overtake the cylinder (one on each side) after impact, move outwards along the wall and experience a weak rebound due to the secondary vorticity generated at the cylinder and wall. At higher Reynolds numbers, this vorticity rolls up into a secondary vortex, which is found to undergo a three-dimensional elliptical instability as it orbits around the primary vortex. This phenomenon eventually leads to the breakdown of the vortex system into small-scale motion.

Comparison between the two-dimensional cylinder configuration and the axisymmetric sphere impact have revealed significant differences. The vortex stretching of the primary vortex, not present for the cylinder case, leads to a reduction in core size and to an accelerated cross-diffusion of the vorticity in the axisymmetric geometry. Both effects delay the inception of three-dimensional instabilities for the flow generated by the impact of a spherical particle on a wall, compared to the two-dimensional counterpart.

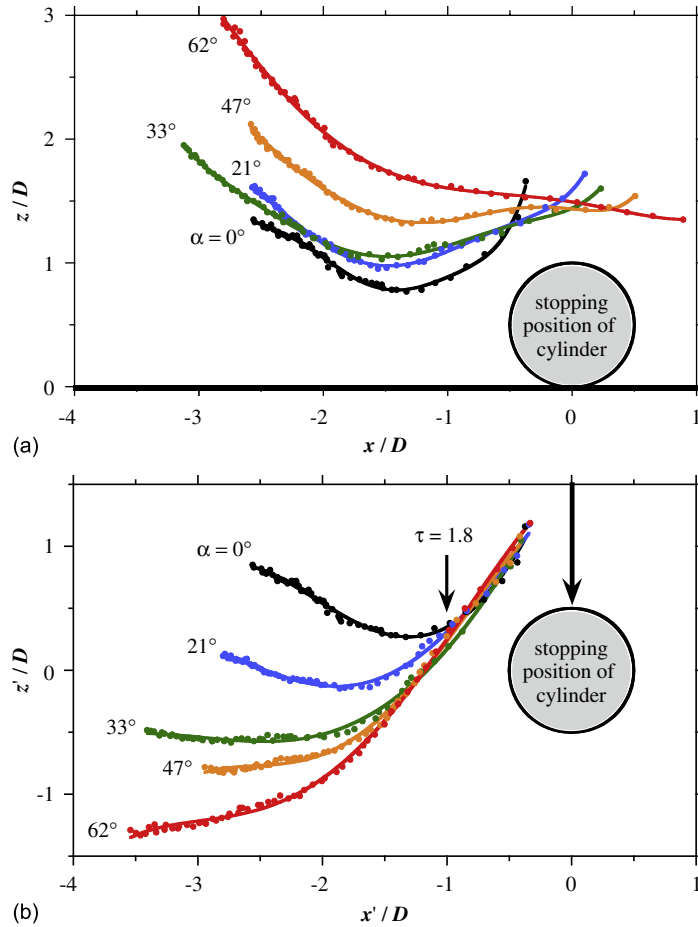


Fig. 7. Experimental trajectories, for different impact angles, of the centre of the primary vortex on the “left” side (“upper” side for oblique impact, see Fig. 6) of the cylinder, for  $Re = 200$  and  $L/D = 4$ . (a) Fixed frame of reference, with the wall at the bottom. (b) Superposition after a rotation of the frame of reference around the cylinder centerline by the respective impact angle. In this representation, the cylinder always moves in the direction of the arrow. The respective wall positions are not shown.

Two-dimensional oblique cylinder impacts at low Reynolds number were also considered. In this asymmetric configuration, the flows generated on both sides of the cylinder are quite different. Whereas the vortical structures on the side underneath the cylinder path are similar to those for normal impact, the wall effect on the opposite side decreases significantly with growing impact angle. Secondary vorticity is only generated at the cylinder surface, leading to the formation of a vortex dipole which induces a rebound of the primary vortex to significantly greater heights than observed for normal impact.

The next step in this line of work is the investigation of oblique sphere impacts. In this configuration, the primary vortex structure in the wake before impact is a vortex ring, i.e., the structures on opposite sides of the body are three-dimensionally connected. Preliminary experimental visualisations have revealed a great complexity of the flow generated in this case, and further analysis is underway.

### Acknowledgements

This research was supported by a Linkage International Grant (no. LX0668992) of the Australian Research Council. Numerical computations were conducted using the resources of the Australian Partnership for Advanced Computing (APAC) National Facility, through the Merit Allocation Scheme.

## References

- Bayly, B.J., 1988. Three-dimensional centrifugal-type instabilities in inviscid two-dimensional flows. *Physics of Fluids* 31, 56–64.
- Eames, I., Dalziel, S.B., 2000. Dust resuspension by the flow around an impacting sphere. *Journal of Fluid Mechanics* 403, 305–328.
- Gondret, P., Lance, M., Petit, L., 2002. Bouncing motion of spherical particles in fluids. *Physics of Fluids* 14, 643–652.
- Karniadakis, G.E., Israeli, M., Orszag, S.A., 1991. High-order splitting methods for the incompressible Navier–Stokes equations. *Journal of Computational Physics* 97, 414–443.
- Kerswell, R.R., 2002. Elliptical instability. *Annual Review of Fluid Mechanics* 34, 83–113.
- Leweke, T., Thompson, M.C., Hourigan, K., 2004. Vortex dynamics associated with the collision of a sphere with a wall. *Physics of Fluids* 16, L74–L77.
- Leweke, T., Thompson, M.C., Hourigan, K., 2006. Instability of the flow around an impacting sphere. *Journal of Fluids and Structures* 22, 961–971.
- Moet, H., 2003. Numerical simulation of the behaviour of wake vortices in the atmosphere. Ph.D. Thesis, Institut National Polytechnique de Toulouse, Toulouse, France (in English).
- Rice, M.A., Willetts, B.B., McEwan, I.K., 1996. Wind erosion of crusted solid sediments. *Earth Surface Processes Landforms* 21, 279–293.
- Ryan, K., Thompson, M.C., Hourigan, K., 2007. The effect of mass ratio and tether length on the flow around a tethered cylinder. *Journal of Fluid Mechanics* 591, 117–144.
- Shao, Y., Raupach, M.R., Findlater, P.A., 1993. Effect of saltation bombardment on the entrainment of dust by the wind. *Journal of Geophysical Research* 98, 12719–12726.
- Sheard, G.J., Leweke, T., Thompson, M.C., Hourigan, K., 2007. Flow around an impulsively arrested circular cylinder. *Physics of Fluids* 19, 083601.
- Thompson, M.C., Hourigan, K., Sheridan, J., 1996. Three-dimensional instabilities in the wake of a circular cylinder. *Experimental Thermal and Fluid Science* 12, 190–196.
- Thompson, M.C., Hourigan, K., Cheung, A., Leweke, T., 2006. Hydrodynamics of a particle impact on a wall. *Applied Mathematical Modelling* 30, 1356–1369.
- Thompson, M.C., Leweke, T., Hourigan, K., 2007. Sphere-wall collisions: vortex dynamics and stability. *Journal of Fluid Mechanics* 575, 121–148.
- Willetts, B., 1998. Aeolian and fluvial grain transport. *Philosophical Transactions of the Royal Society London A* 356, 2497–2513.
- Zhang, J., Fan, L.-S., Zhu, C., Pfeffer, R., Qi, D., 1999. Dynamic behavior of collision of elastic spheres in viscous fluids. *Powder Technology* 106, 98–109.
- Ziskind, G., 2006. Particle resuspension from surfaces: revisited and re-evaluated. *Reviews in Chemical Engineering* 22, 1–123.